THE JOURNAL OF BIOLOGICAL CHEMISTRY
Vol. 275, No. 44, Issue of November 3, pp. 34335–34343, 2000

Printed in U.S.A.

Structural Characterization of the Catalytic Active Site in the Latent and Active Natural Gelatinase B from Human Neutrophils*

Received for publication, June 29, 2000
Published, JBC Papers in Press, August 9, 2000, DOI 10.1074/jbc.M005714200

Oded Kleifeld‡, Philippe E. Van den Steen§¶, Anatoly Frenkel‖, Feng Cheng‡‡§§, Hua Liang Jiang‡‡§§, Ghislain Opdenakker§¶, and Irit Sagi‡¶¶**

From the ‡Department of Structural Biology, The Weizmann Institute of Science, Rehovot 76100, Israel, the §Rega Institute for Medical Research, University of Leuven, Laboratory of Molecular Immunology, Minderbroedersstraat 10, B-3000 Leuven, Belgium, the ‖Materials Research Laboratory, University of Illinois, Urbana-Champaign, Urbana, Illinois 61801, and ‡‡State Key Laboratory of Drug Research, Shanghai Institute of Meteria Medica, Chinese Academy of Sciences, 294 Taiyuan Road, Shanghai 200031, China

Matrix metalloproteinases are endopeptidases that have a leading role in the catabolism of the macromolecular components of the extracellular matrix in a variety of normal and pathological processes. Human gelatinase B is a zinc-dependent proteinase and a member of the matrix metalloproteinase family that is involved in inflammation, tissue remodeling, and cancer. We have conducted x-ray absorption spectroscopy, atomic emission, and quantum mechanics studies of natural and activated human gelatinase B. Our results show that the natural enzyme contains one catalytic zinc ion that is central to catalysis. In addition, upon enzyme activation, the catalytic zinc site exhibits a conformation change that results in the expansion of the bond distances around the zinc ion and the replacement of one sulfur with oxygen. Interestingly, quantum mechanics calculations show that oxygen ligation at the catalytic zinc ion exhibits a greater affinity to the binding of an oxygen from an amino acid residue rather than from an external water molecule. These results suggest that the catalytic zinc ion plays a key role in both substrate binding and catalysis.

Remodeling of the extracellular matrix is an important event in many normal and pathological processes such as growth, wound repair, tumor metastasis, and leukocyte mobilization in inflammation. A large family of zinc-dependent proteinases, the matrix metalloproteinases (MMPs),[1] is considered to be primarily responsible for this matrix catabolism (1–4). Details of their variety and substrate specificity are documented in several recent reviews (5–7). The MMPs consist of a large family of proteinases that share many common structural and functional elements. MMPs can be categorized based on amino acid sequence similarity, substrate specificity, and domain structure. They include collagenases, which cleave triple helical interstitial collagens; gelatinases, which cleave denatured collagen, elastin and type IV and V collagens; stromelysins, which mainly cleave proteoglycans; and membrane-type MMPs, which are associated with the activation of pro-MMPs (2, 3). In addition to these classical MMPs, other metalloproteinases, mainly with functions other than matrix catabolism, are being discovered at an increasing pace.

All MMPs are synthesized as preproenzymes and are usually secreted as inactive pro-MMPs. The primary structure of each MMP is composed of some of the following domain motifs: a signal peptide, a propeptide, a catalytic domain that contains a zinc ion central to catalysis, a linker, a hemopexin-like domain, a fibronectin type II domain, a transmembrane region and a cytoplasmic domain (found in membrane-types 1–6), a furin-recognition sequence, and a vitronectin-like domain (7). Moreover, each member of the MMP family is characterized by a different domain composition, but contains a propeptide domain of about 80 amino acids with a conserved PRCGVPDV motive that ligates to the catalytic zinc ion via the cysteine residue to maintain the latency of the proenzyme (8, 9). The catalytic domain (about 170 amino acids) contains a zinc-binding motive HE*XX*H*XX*G*XX*H, and all MMPs except MMP-7 have a hemopexin-like domain (about 210 amino acids) at the carboxyl terminus. The hemopexin-like domain is reported to be required for the digestion of native collagen by collagenase-1, -2, and -3 as well as for the binding of TIMP-1 to progelatinase B and TIMP-2 to progelatinase A (10).

The first x-ray crystal structures of the recombinant catalytic domains of human fibroblast collagenase/MMP-1 (11) and human neutrophil collagenase/MMP8 (12) were soon complemented by additional structures of catalytic domains, full-length recombinant enzymes, and inhibitor-enzyme complex structures (9, 13–17). Importantly, these detailed atomic resolution structures have revealed the location of the conserved motifs and have enabled the assignment of substrate recognition sites on the proteinases. The catalytic domains of the MMPs have an ellipsoid shape with a small active site cleft on their surfaces. This cleft contains the catalytic zinc atom. Several studies have suggested that the catalytic domain of the isolated MMPs contains two zinc atoms (11, 18, 19) that are required for enzyme stabilization and catalysis. To date, how-

* This work was supported in part by Grant 6602/2 from the Bi-National Scientific Foundation and the Maurizìo and Clotilde Pontecorvo Fund. The costs of publication of this article were defrayed in part by the payment of page charges. This article must therefore be hereby marked "*advertisement*" in accordance with 18 U.S.C. Section 1734 solely to indicate this fact.

¶ Supported by Fortis Insurances A.B., Belgium, and the F. W. O. -Vlaanderen.

** Supported by Department of Energy Grant DEFG02-96ER45439 through the Materials Research Laboratory at the University of Illinois at Urbana-Champaign. Mailing address: Bldg. 510 E, Brookhaven National Laboratory, Upton, NY 11973.

§§ Supported by the National Natural Science Foundation of China Grant 29725203 and the State Key Program of Basic Research of China Grant 1998051115.

¶¶ To whom correspondence should be addressed: Dept. of Structural Biology, The Weizmann Institute of Science, P. O. Box 26, Rehovot 76100, Israel. Tel./Fax: 972-8-934-2130; E-mail: irit.sagi@weizmann.ac.il.

[1] The abbreviations used are: MMPs, matrix metalloproteinases; XAS, x-ray absorption spectroscopy; DFT, density functional theory; ICP-AES, inductively coupled plasma atomic emission spectroscopy; EXAFS, extended x-ray absorption fine structure; XANES, x-ray absorption, near edge structure.

ever, none of these structural studies have dealt with natural or intact MMP-9. Recent reports and our results (reported here) suggest that the intact full-length MMPs contain only a single zinc atom. Together, these discrepant results suggest that the second zinc-binding site may result from a molecular rearrangement and subsequent structural stabilization due to truncation of the polypeptide chain (20, 21). The crystal and NMR structures of the various MMPs provide a framework for the design of mechanistic studies. However, the actual mechanism of MMP catalysis has yet to be elucidated.

Previous studies led to the formulation of the "cysteine switch hypothesis" as a model for understanding the unique structure of MMP zymogens and the means by which activation may be achieved *in vitro* (8). Briefly, the cysteine switch model suggests that upon activation, the latent zinc-binding site is converted to a catalytic zinc-binding site by dissociation of the thiol-bearing propeptide from the zinc atom. Cleavage of the propeptide results in a breakdown of the prodomain structure of the enzyme, and the shielding of the catalytic zinc ion is withdrawn. Consequently, the metal ion and the active site pocket are accessible for substrate binding (22).

Human gelatinase B is a matrix metalloprotease (MMP-9) involved in inflammation, tissue remodeling, development, and cancer (23, 24). Importantly, this MMP is a marker of inflammatory diseases, including rheumatoid arthritis and multiple sclerosis (25, 26). In the central nervous system, gelatinase B may play a role in the enzymatic degradation of the blood-brain barrier and may generate autoimmune peptides from intact myelin constituents, suggesting that it may be at the basis of autoimmunity in multiple sclerosis (27). By analogy with other proteases (28), it has also been suggested that the secretion of gelatinase B may play a key role in tumor cell metastasis by providing the basis for the mechanism of extracellular matrix remodeling (29, 30). Human neutrophils produce three major forms of pro-gelatinase B as follows: 92-kDa monomers, homodimers, and complexes of gelatinase B covalently bound to neutrophil gelatinase B-associated lipocalin (31). Gelatinase B is not produced constitutively by most cells, but instead its activity is induced by different stimuli depending on the cell type, thus providing a means of increasing the local concentration of gelatinolytic activity in response to specific physiological events. Therefore, it is considered to be one of the most complex MMPs in terms of regulation and expression, in addition to possessing a complex domain structure (23, 24, 31–33). Recently it was reported that glycosylation of the gelatinase B molecule is considerable in terms of molecular volume, but the function of this post-translational modification is as yet not clear (31). Therefore, further structural analysis of the catalytic site of the full-length natural human gelatinase B may contribute to understanding its mode of action.

Here we report on our x-ray absorption spectroscopy (XAS) studies of the catalytic active site of natural human gelatinase B in its latent and activated states. The XAS results are consistent with the density functional theory (DFT) calculations on the active sites of MMPs in latent and activated forms, which are also reported here. Our results demonstrate the molecular rearrangement and conformational changes that occur upon activation in human gelatinase B at the zinc site. In addition, we show by independent experimental procedures that natural human gelatinase B contains one zinc atom.

EXPERIMENTAL PROCEDURES

Purification of Natural Gelatinase B from Human Neutrophils to Homogeneity

Natural gelatinase B was isolated from human neutrophils by using a method modified from Masure *et al.* (24). Human neutrophils were isolated from buffy coats (Red Cross, Antwerp, Belgium) (34). After a 20-min preincubation with 3 mM phenylmethylsulfonyl fluoride at 37 °C, 0.5 μM formyl-methionyl-leucyl-phenylalanine and 3 mM phenylmethylsulfonyl fluoride were added to stimulate degranulation for the next 20 min. The cell supernatants were harvested, filtered, loaded on a gelatin-Sepharose substrate affinity column (Amersham Pharmacia Biotech), and eluted as described (24). The eluate was then dialyzed against assay buffer (100 mM Tris-HCl, pH 7.5, 100 mM NaCl, 10 mM $CaCl_2$, 0.01% Tween 20). In the next step, the covalent heterodimeric complex of gelatinase B with neutrophil gelatinase B-associated lipocalin was removed by affinity chromatography on a monoclonal antibody directed against neutrophil gelatinase B-associated lipocalin, courtesy of Dr. T. Bratt and Dr. N. Borregaard (35). The purity of gelatinase B was controlled by reducing and non-reducing SDS-polyacrylamide gel electrophoresis and analyzed by Coomassie Brilliant Blue protein staining.

Protein Concentrations

Protein concentration was determined using a Bradford reagent (Bio-Rad) (36) with bovine serum albumin as a standard and according to amino acid composition analysis. The active site of gelatinase B was titrated using different concentrations of recombinant human TIMP-1 (Calbiochem) in an enzyme activity assay with a fluorogenic peptide, as described by Knight *et al.* (37).

Enzyme Activity Assay

The enzyme samples and the appropriate controls were analyzed by gelatin substrate zymography (38). This technique provides information about the molecular size and the catalytic activity of the enzyme. Gelatinase B activity was measured and quantified by the conversion of a fluorogenic peptide (37).

Inductively Coupled Plasma Atomic Emission Spectroscopy (ICP-AES)

The metal content in gelatinase B samples was analyzed by inductively coupled plasma atomic emission spectroscopy using the ICP-AES model "Spectroflame" from Spectro (Kleve, Germany). Prior to measurement, the samples were digested with nitric acid, and the volume was adjusted to 6 ml (final concentration 10%). The zinc content in the protein samples was determined relative to an equivalent amount of gelatinase assay buffer.

X-ray Absorption (XAS)

Sample Preparation—Enzymatic activity was checked for all samples by zymography and by the conversion of the fluorogenic peptide before XAS data collection. The enzyme was concentrated by ultrafiltration using a Millipore Centricon-30 (Bedford, MA) apparatus to make a final concentration of 70 μM (6.4 mg/ml). Samples were loaded into copper sample holders ($10 \times 5 \times 0.5$ mm) covered with Mylar tape and were frozen immediately in liquid nitrogen. The frozen samples were then mounted inside a Displex closed cycle helium cryostat and their temperature was maintained at 30 K to minimize the thermal disorder in the XAS data.

Data Collection—XAS data collection was performed at the National Synchrotron Light Source at Brookhaven National Laboratory, beam line X9B. The spectra were recorded at the zinc K-edge in fluorescence geometry at low temperature (30 K). The beam energy was defined using a flat silicon(111) monochromator crystal. The incident beam intensity I_0 was recorded using an ionization chamber. The fluorescence intensity was recorded using a 13-element germanium detector. The transmission signal from a zinc foil was measured with a reference ion chamber simultaneously with fluorescence in order to calibrate the beam energy. Several scans of each sample were collected for a total of 1×10^6 counts across the edge. The samples were checked for burning marks after each scan, and the beam position on the sample was changed before each scan to minimize radiation damages. Enzyme activity was checked after exposure to x-rays, and the enzyme was found to be fully active.

Data Processing and Analysis—The average zinc K-edge absorption coefficient $\mu(E)$, which was obtained after several independent XAS measurements for each sample, was aligned in absolute energy, using the reference zinc metal foil XAS data as an absolute energy calibrant. Subsequently, the absorption coefficients for different samples were shifted in x-ray energy until their first inflection points were aligned at the same energy (9658 eV). This alignment ensured, to a good approximation, that the same x-ray energy, $E_0 = 9658$ eV could be used as the photoelectron energy origin in all data sets.

The smooth atomic background was removed with the AUTOBK

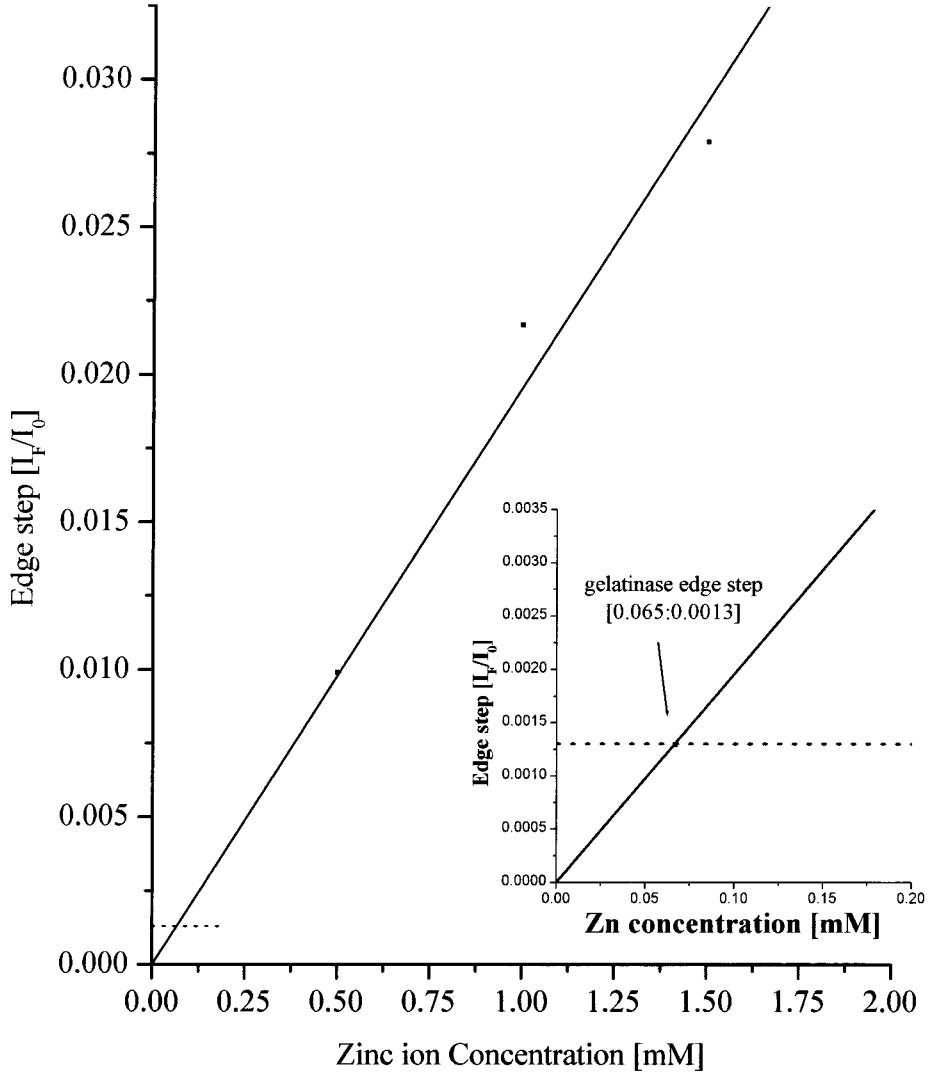

FIG. 1. **Edge-step analysis of natural human gelatinase B.** The edge intensity of human gelatinase B is compared with the standard calibration curve. Proteins and standards were measured and processed with identical procedures. The zinc:enzyme ratio is consistent with 1:1 stoichiometry.

program of the UWXAFS data analysis package, developed at the University of Washington, Seattle (39). The same energy, E_0 = 9658 eV, was chosen for the purpose of background removal as the origin of the photoelectron energy. The R space region for minimizing the signal below the first shell was chosen between 1 and 1.2 Å. After the removal of background, the useful k range in the resultant k^2 weighted $\chi(k)$ was between 2.5 and 9 $Å^{-1}$. Model data for the fitting procedure were constructed by extracting the catalytic zinc site coordinates (in a radius of 6 Å) from the crystallographic coordinates of stromelysin-1 (MMP-3) derived from the protein data bank (code 1SLM) (9), gelatinase A (protein data bank code 1CK7), and the optimized active site structures obtained from our quantum mechanical calculations. By using the computer code FEFF7 (41, 42), we calculated the theoretical photoelectron scattering amplitudes and phase shifts. Total theoretical $\chi(k)$ was constructed by adding the most important partial $\chi(k)$s that contributed to the r range of interest.

The theoretical XAFS signal was fitted to the experimental data using the non-linear least squares method, implemented in the program FEFFIT (39) in R space, by Fourier transforming both theory and data. Data and theory were weighted by k and multiplied by a Hanning window function in Fourier transforms.

Quantum Mechanics Calculation Methods

The DFT computational method B3LYP was applied on a model of the first coordination shell around the catalytic zinc ion in the MMPs. The B3LYP/3-21G method was employed for full optimization of the initial model structures, and the optimized structures were then subjected to further optimization with B3LYP/6-31G*. Based on the optimized geometries, the frequency calculations were carried out at the B3LYP/6-31G* level of theory in order to verify the accuracy of the optimized structures and to determine the zero point and vibrational energies, enthalpy, and entropy parameters. All quantum mechanic calculations were carried out with the Gaussian98 program (44).

RESULTS

The active site structures of the catalytic zinc ion in natural gelatinase B from neutrophils, in its latent and activated states, were studied by x-ray absorption, near edge structure (XANES), and extended x-ray absorption fine structure (EXAFS) spectroscopy. EXAFS is a valuable technique for elucidating the structure of a variety of metal sites in metalloproteins (45). More specifically, EXAFS measures the transition from the core electronic states of the metal to the excited electronic or continuum states. Spectral analysis near the electronic transition (XANES) provides information about the charge state of the metal and its geometry. Spectral analysis above the absorption edge, in the EXAFS region, provides complementary structural information such as coordination numbers, types, and distances from neighboring atoms to the central (absorbing) atom. In addition, XAS is an excellent structural tool to probe the d^{10} zinc ion, which is generally spectroscopically silent (46). We therefore conducted XAS studies to examine the nature and bonding of active site ligands and the changes in metal site structures upon activation of human gelatinase B. Furthermore, EXAFS analysis was used to examine the zinc stoichiometry in human gelatinase B.

Determination of Zinc Content in Human Gelatinase B from Neutrophils—For fixed geometry of the fluorescence EXAFS

experiment, the edge step of the x-ray absorption coefficient should be proportional to the concentration of the absorbing element. Therefore, the number of zinc atoms per protein can be determined by comparing the edge-step intensity measured in the enzyme absorption coefficient data with the calibration curve obtained for standard compounds, where the edge step is measured as a function of the zinc concentration. Aqueous solutions in the range of 0.5–1.5 mM of $ZnCl_2$ were chosen as standard compounds for the purpose of edge intensity calibration. The calibration curve presented in Fig. 1 shows a linear relationship between the edge- step intensity changes and the function of increasing zinc ion concentration (linearity in the lower concentrations of the calibration curve was obtained by linear extrapolation to zero). The enzyme concentration was independently obtained to be 0.07 mM by conducting an amino acid analysis experiment, a standard Bradford assay, and by titration of the active enzyme with TIMP-1 (see "Experimental Procedures"). To obtain the estimated concentration of zinc ion in the enzyme as measured by XAS, we crossed the experimental edge-step intensity value of gelatinase B with the calibration curve. The concentration of zinc ion obtained by this type of analysis was 0.065 mM which is consistent with one zinc atom per enzyme (Fig. 1). These results were repeated using different protein preparation batches and different germanium detectors in measuring the XAS. Since the edge-step analysis may deviate from linearity because of detector limitation at very low concentrations, we further examined the zinc stoichiometry by ICP-AES.

The atomic absorption signal of the enzyme was measured and placed on a standard calibration curve, which was obtained by measuring standards of known zinc concentrations in the range of 0–1000 parts/billion. The zinc content of the buffer solution was 2 parts/billion. The enzyme was diluted by a factor of 240 before measuring the atomic absorption. The zinc concentration in the enzyme was 17 parts/billion, which is equivalent to 62 μM in the zinc concentration (the enzyme concentration was 70 μM as described). These results show that the zinc content in the enzyme is consistent with one zinc ion per enzyme in a ratio of 0.89:1 zinc to protein and were found to be in good agreement with our edge-step analysis. The presence of single as opposed to multiple zinc sites simplifies the EXAFS data analysis procedure, since the curve-fitting analysis of the local environment around the multiple zinc ions requires an excessive number of structural variables in the analysis. However, we further examined the possibility of the contribution of multiple zinc atoms by non-linear curve-fitting EXAFS analysis to be detailed.

EXAFS Analysis—EXAFS analysis of human gelatinase B, in its latent and activated forms, was conducted by fitting the data to theoretical phase shifts and amplitudes. Theoretical models of the proposed structural and catalytic zinc sites were constructed from the crystal structure of MMP-3 (9), gelatinase A (MMP-2) (22), and our calculated model (see Table II). The architecture of the catalytic domain, known as the matrixin fold (47), is highly conserved in MMPs and is unaffected by insertion of the fibronectin domains (22). The vicinity of the binding sites of the catalytic and the structural zinc ions reported in the crystal structure of pro-MMP2 are identical to those of pro-MMP3, respectively (22). Although human gelatinase B shows a greater sequence homology to gelatinase A (MMP-2), we chose to use the structural coordinates of the zinc site in both structures in order to examine our fitting procedure by various models. The catalytic zinc ion in the MMP-3 proenzyme is bound to three histidines and one cysteine, and the structural zinc ion is bound to three histidines and one aspartate (22). The theoretical models that were constructed from these sites were used to modulate the zinc site in human gelatinase B before and after activation. Fig. 2*a*—*c* shows the fitting results of pro-gelatinase B with both models, and the quality of the fits are presented in Table I, part a. The zinc site in human gelatinase B was fitted to the Zn-N, Zn-O, Zn-S, and Zn-C paths using different combinations of varied and constraint parameters together with starting the fits from different initial conditions of distances, Debye-Waller parameters, and ΔE_0 shifts. Stable and reproducible fits of the latent enzyme were consistent with a tetrahedral coordination of the zinc ion with three Zn-N at 1.83 ± 0.01 Å, one Zn-S at 2.24 ± 0.01 Å, and seven Zn-C at 2.87 ± 0.01 Å contributions in the first and second coordination shells. All attempts to fit the catalytic zinc ion in the latent enzyme to four Zn-N/O or three Zn-N and one Zn-O contributions failed or resulted in high Debye-Waller factors and unreasonable χ^2 values (Fig. 2, *b* and *c,* and Table I; Fits 2 and 3).

In addition, we have used the partial contributions of Zn-O (Asp) and Zn-S (Cys) in the same fit to examine sample homogeneity and any contribution from putative structural zinc. The results obtained from this model with a fixed 1:1 ratio between the Zn-S and Zn-O contributions were unstable with high χ^2 and Debye-Waller factors (see Table I part a, Fit 3). Simultaneous fits of latent gelatinase B to this model with a varied ratio between the Zn-O and Zn-S contributions were consistent with three Zn-N ligands with an average bond distance at 1.87 ± 0.04 Å and one Zn-S bond distance at 2.25 ± 0.05 Å for the latent enzyme. Any attempts to eliminate the Zn-S contribution or, alternatively, add a partial Zn-S path in the fitting analysis of the latent enzyme failed (data not shown). These results are consistent with our atomic absorption and XAS edge-step studies, which support one catalytic zinc ion in human gelatinase B.

A similar curve-fitting procedure was applied in analyzing activated human gelatinase B. Fig. 3 shows the best fitting results of the activated enzyme. Table I, part b, lists the quality and the fitting parameters. Best fits were obtained using the structural zinc site in MMP-3 as a model ($Zn(His)_3(Asp)_1$). This model provides 3 Zn-N, 1 Zn-O, and 7 Zn-C theoretical paths. Fitting experimental data to this model resulted in 3 Zn-N at 2.00 ± 0.01 Å, 1 Zn-O at 1.78 ± 0.02 Å, and 6 Zn-C at 2.59–2.97 ± 0.02 Å bond distances (see Table I, part b). In these fits the Zn-N contributions were constrained to one path. Fitting the catalytic zinc ion in the activated enzyme to the three different Zn-N paths resulted in similar Zn-ligand distances and similar fit quality. This means that the distance spread of the three Zn-N contributions is small and cannot be resolved by EXAFS. All attempts to fit the experimental data to the ($Zn(His)_3(Cys)_1$) model or, alternatively, to partial Zn-S contributions failed.

Structural changes that result from the activation of pro-gelatinase B can be observed in the raw XAS data. Fig. 4 shows the raw x-ray fluorescence data at the XANES region. The normalized spectra of the pro- and the activated forms of the enzyme exhibit a significant change in edge shape upon enzyme activation. Changes in peak intensities are observed at 9680, 9710, and 9739.5 eV. Alternation in the shape of the structural features at the XANES region upon enzyme activation can be attributed to the cleavage of the propeptide and the substitution of the sulfur with the oxygen contribution at the active site. In addition, a moderate edge shift (0.3 eV) to a higher energy is observed upon enzyme activation. This may indicate that the total atomic charge of the zinc ion does not change substantially as observed by our quantum mechanics calculations (Table II, part b). The effect of electron donation by various ligands at the catalytic zinc ion in the MMPs is

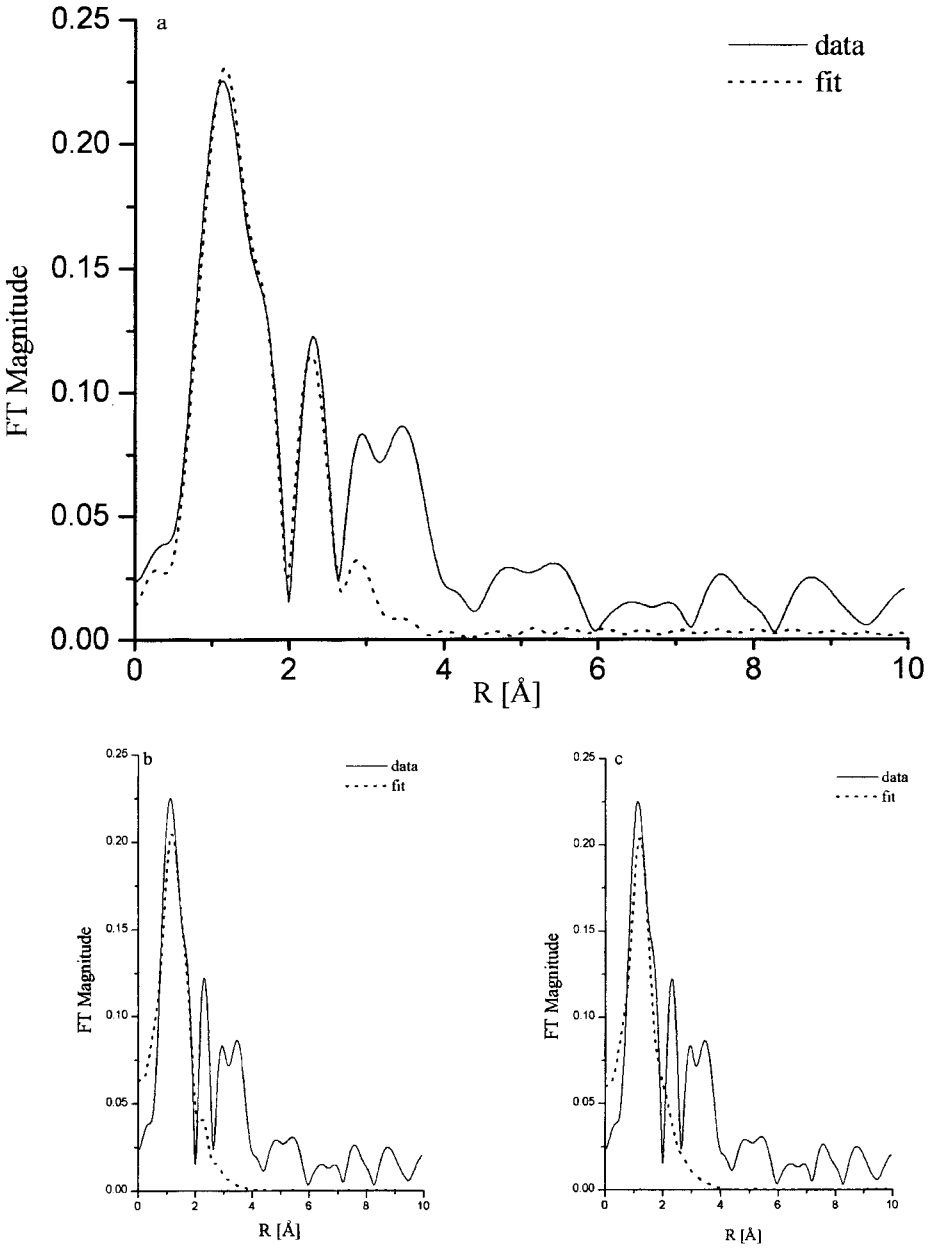

FIG. 2. **EXAFS-fitting results of the catalytic zinc site in pro-human gelatinase B.** The results are presented in the *R* space of the experimental data (*solid line*) of pro-human gelatinase B to simulated theoretical Zn-ligand contributions (*dotted line*). The experimental data were extracted and normalized using the UWXAFS analysis package. The theoretical XAFS signal was constructed based on protein data bank and our optimized structures (calculated by DFT and processed using FEFF7). The experimental data were fit to the theoretical data using the non-linear least squares method implemented in the program FEFFIT in *R* space, by Fourier transforming both theory and data. *a,* best fit of pro-gelatinase B to a single zinc site with three Zn-N, one Zn-S, and seven Zn-C contributions. *b,* fitting results of pro-gelatinase B to two zinc sites (simulation of 3 Zn-N, 0.5 Zn-O, and 0.5 Zn-S contributions). *c,* fitting results of pro-gelatinase B to 3 Zn-N and 1 Zn-S contributions. *b* and *c* demonstrate the poor results that were obtained by this type of analysis. The fitting parameters are listed in Table I, part a.

discussed next.

Quantum Mechanics Calculations—DFT has recently been recognized as an efficient quantum chemistry method for studying molecular properties at the atomic and electronic levels (48). The hybrid density functional method B3LYP (49), a DFT computational method, has been shown to be an accurate density functional method (50, 51), giving as good or better geometries and energies as correlated *ab initio* methods for first-row transition metal complexes (50–53). To complement our EXAFS analysis we applied B3LYP to various relevant models of the catalytic zinc site in the MMPs.

The typical zinc coordination sphere in MMPs consists of three histidine (His) residues and one exogenous ligand. For the quantum mechanics calculations the histidine residues were modeled by imidazoles, and the active site of the MMPs was modeled by ZnX_3Y, where X is imidazole and Y is exogenous ligand. As for the exogenous ligands, we investigated three typical cases as follows: acetate (model 1), water (model 2), and methane thiol (model 3), which mimic aspartate or glutamate, catalytic water, and cysteine, respectively (Scheme 1). The initial structure of model 1 was isolated from the x-ray crystallographic structure of fibroblast stromelysin-1 (protein data bank entry 1SLM) (9), and the initial structures of models 2 and 3 were constructed by substituting the acetate of the optimized geometry of model 1 with a water molecule and methane thiol, respectively.

Table II shows the results of the charge population analysis in the form of atomic and group charges of each complex. The group charge is calculated by the summing over all the atomic charges of the atoms that compose the group. An increase in the group charge indicates that an electron transfer from the ligands to the zinc ion has occurred and that the coordination bond has formed. The group charges of acetate, water, and methane thiol in the free status are −1.0, 0.0, and 0.0 *Q/e*, respectively, and those in the complexes are −0.531, 0.165, 0.251 *Q/e* (B3LYP/6-31G* result), respectively. However, the change in atomic charge is different for these three complexes. As shown in Table II, the atomic charges of the zinc-bound atoms, O-2 and O-19 in acetate, and O-2 in water and S-2 in methane thiol, increase in model 1 (from −0.640 *Q/e* to −0.600 *Q/e* for O-2 and from −0.639 *Q/e* to −0.579 *Q/e* for O-19 atom) and in model 3 (from −0.08 *Q/e* to −0.035 *Q/e* for atom S-2).

TABLE I
Curve-fitting analysis of human gelatinase B

Results of simultaneous EXAFS curve-fitting analysis of pro (a) and activated human gelatinase B (b). The uncertainties are given. The symbols F and V stand for fixed and varied and indicate how the respective parameter was treated in the fit model. R is distance of atoms from the zinc atom (in Angstroms). σ^2 is the Debye-Waller factor.

Fit	Reduced χ^2	Path	ΔE_0	R	σ^2
				Å	
a. Latent gelatinase B					
Fit 1	9	Zn-N X3	−2.5 (F)	1.83 ± 0.01 (V)	4E-3 (V)
		Zn-S X1	−2.5 (F)	2.24 ± 0.01 (V)	1E-6 (V)
		Zn-C X7	−2.5 (F)	2.87 ± 0.01 (V)	6E-3 (V)
Fit 2	141	Zn-N X3	−5 (F)	1.80 ± 0.07 (V)	7E-3 (V)[a]
		Zn-O X1	−5 (F)	2.00 ± 0.25 (V)	1E-6 (V)[a]
		Zn-C X7	−5 (F)	2.71 ± 0.18 (V)	3E-2 (V)[a]
Fit 3	128	Zn-N X3	−6 (F)	1.79 ± 0.14 (V)	6E-3 (V)[a]
		Zn-O X0.5	−6 (F)	1.97 (F)	4E-6 (V)[a]
		Zn-S X0.5	−6 (F)	2.22 ± 0.49 (V)	1E-6 (V)[a]
		Zn-C X6	−6 (F)	2.73 ± 0.33 (V)	2.7E-2 (V)[a]
Fit 4	13.3	Zn-N X3	−2.3 (F)	1.87 ± 0.01 (V)	3E-3 (V)
		Zn-S X1	−2.3 (F)	2.27 ± 0.01 (V)	1E-6 (V)
		Zn-C X7	−2.3 (F)	2.89 ± 0.01 (V)	4E-3 (V)
Fit 5	8	Zn-N X3	3.5 (F)	1.84 ± 0.01 (V)	6E-3 (V)
		Zn-S X1	3.5 (F)	2.23 ± 0.01 (V)	1E-6 (V)
		Zn-C X7	3.5 (F)	2.87 ± 0.01 (V)	6E-3 (V)
	Reduced χ^2	Path	ΔE_0		
b. Active gelatinase B					
Fit 6	3.9	Zn-NX3	4.2 (F)	1.83 ± 0.01 (V)	4E-3 (V)
		Zn-OX1	4.2 (F)	2.24 ± 0.01 (V)	1E-6 (V)
		Zn-CX6	−4.0 (F)	2.87 ± 0.01 (V)	6E-3 (V)
Fit 7	0.89	Zn-NX3	1.3 (F)	2.00 ± 0.01 (V)	2E-3 (V)
		Zn-OX1	1.3 (F)	1.78 ± 0.02 (V)	1E-6 (V)
		Zn-C1X3	1.3 (F)	2.59 ± 0.02 (V)	4E-3 (V)
		Zn-C2X4	1.3 (F)	2.97 ± 0.02 (V)	4E-3 (V)

[a] Results are with very high uncertainties of σ^2.

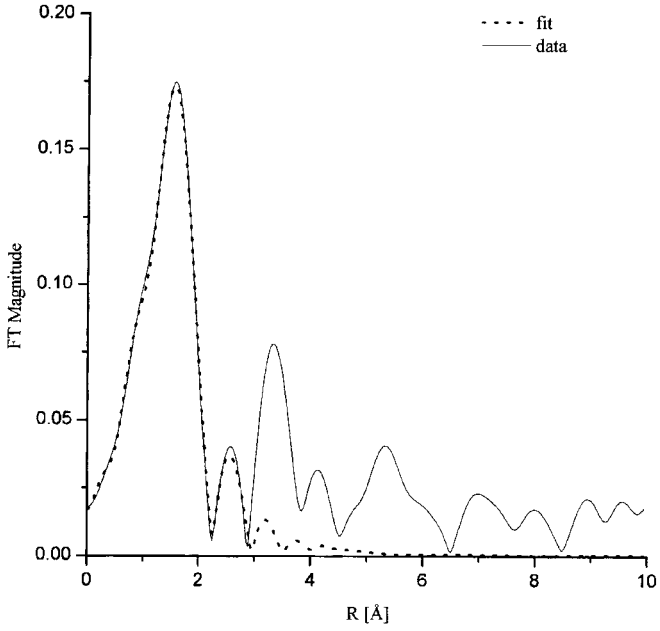

FIG. 3. **Curve-fitting results of activated human gelatinase B.** Representation in R space of the best fitting results of activated human gelatinase B. The fitting parameters are listed in Table I, part b. The best fit is consistent with three Zn-N and 1 Zn-O contributions.

However, the atomic charge of coordinated O-2 in model 2 is more negative (from −0.774 Q/e to −0.789 Q/e for O-2).

The increase in electron density of the oxygen atom of water makes the water more active as a nucleophile. Interestingly, our thermodynamic parameter analysis (Table II) indicates that the order of decreasing binding ability of the various ligands to zinc is in the order acetate ≫ water > methane thiol. These results were obtained by calculating the free energy change of ligand exchange of a virtual reaction at the catalytic zinc ion. Table II presents the theoretical results of internal energies (E_y), thermal energies (E_{therm}), and entropies (S) of the three complex models calculated by B3LYP at the 6–31G* basis set level. As shown in Table II, the free energy change in substituting acetate with water is −191.06 kcal/mol and for substituting methane thiol with water is 7.75 kcal/mol.

Table II also shows the bond lengths of the optimized structures of the model molecules. The optimized values of the coordination bonds of the various models are generally in agreement with the results derived from B3LYP at the double-ζ basis set level (51). The bond distances obtained by EXAFS analysis compared with those obtained by the B3LYP calculation indicate that the Zn-O and Zn-N distances are in good agreement within the experimental error. In contrast, the cal-culated Zn-S distance, obtained by B3LYP, appears to be longer than the experimental distance.

DISCUSSION

In this work we present the local structure of the active zinc site in natural human gelatinase B from neutrophils. The structure of the zinc coordination environment was studied in both the latent and the activated forms of the enzyme using EXAFS spectroscopy and complementary quantum mechanics calculations. In addition, we address the controversial issue of zinc content per enzyme molecule.

Several high resolution molecular structures clearly showed that the isolated catalytic domain of the MMPs contains two zinc ions (11–13, 17–19). A structural role has been proposed for the second zinc ion on the basis of its location in the protein

structure and its high affinity for the protein. Although crystallographic data provide evidence for two zinc ions in MMPs, direct stoichiometry analysis of the zinc content of these enzymes gave results of zinc contents that varied between one and two metal atoms per enzyme (21, 55). Willenbrock *et al.* (21) and Springman *et al.* (55) have questioned the existence and the necessity of a second zinc ion for enzyme catalysis. Their studies suggested that full-length metalloenzymes may contain one catalytic zinc ion and that the enzyme is stabilized by the protein side chains themselves or by calcium ion concentrations.

Our results show that natural and activated human gelatinase B contains one zinc ion per enzyme. The zinc content of the natural full-length and glycosylated human gelatinase B was determined independently by atomic absorption, XAS edge-step, and EXAFS analysis. These results question the enzyme requirement for an additional zinc ion for enzyme catalysis. Therefore, we propose that the second zinc ion, which was found in other MMPs, may provide a stable structural conformation of the enzyme by specifically binding to a high affinity "zinc-binding" site in the enzyme.

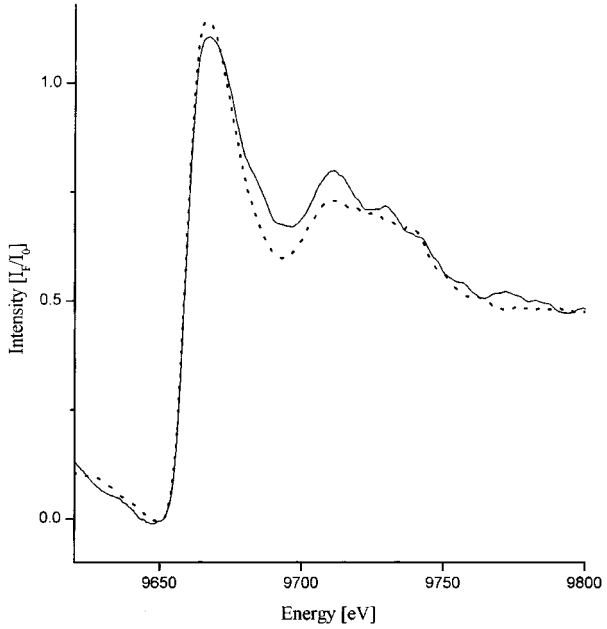

FIG. 4. **Edge spectra of pro- and activated forms of human gelatinase B.** Raw XAS data in the zinc K-edge region of pro-human gelatinase B (*solid line*) and activated human gelatinase B (*dotted line*). All data sets were normalized by fitting a linear polynomial function −150 to −20 eV and 75–200 eV below and above the edge, respectively. The edge step was determined by the difference between the pre-edge and post-edge fits. The overall shape of the edge spectra of the pro- and activated enzyme differs. The most distinct features are the edge shape changes of the peaks at 9680, 9710, and 9729.5 at the XANES region. In addition, a moderate edge shift (0.3 eV) to a lower edge energy can be observed for the activated enzyme.

The EXAFS curve-fitting analysis of the catalytic zinc site in the proenzyme and activated enzyme provides direct evidence that the well accepted "cysteine switch" mechanism in MMPs (8) applies to natural human gelatinase B. Structurally, the proenzyme zinc site is characterized by tetrahedral coordination of the zinc ion, which is consistent with three Zn-N(His) and one Zn-S(Cys) ligands, and the activated enzyme is consistent with three Zn-N(His) and one Zn-O ligands. These results demonstrate that the structure of the catalytic zinc site in human gelatinase B is altered upon enzyme activation by releasing the sulfur "blockage." The new "unlocked" conformation results in a slight expansion of the zinc coordination shell, structural distortion, and replacement of the Zn-S with Zn-O contribution. We have assigned the oxygen ligand in the activated enzyme to a water molecule.

The presence of a water molecule as the fourth ligand in the activated form of MMPs was suggested previously by several studies (1, 13, 47, 56, 57). The crystal structures of the various proenzyme MMPs clearly show that solvent molecules can be accessible to the catalytic zinc ion only after cleavage of the propeptide is achieved. Interestingly, Vallee and Auld (40) pointed out that the mechanism of activation of zinc-bound water in catalytic sites of zinc enzymes is dependent on the identity of the other three ligands and their spacing. "Short spacers" (1–3 amino acids) provide the proximity of protein residues and may facilitate the formation of a primary bidentate zinc complex. In contrast, "long spacers" provide flexible geometries at the zinc ion coordination site and allow the accommodation of a substrate or product molecule to interact during catalysis. Comparative sequence analysis of various MMPs reveals that the catalytic binding domain includes the consensus sequence H*EXXHXXGXX*H, which is the zinc-binding motif (2, 3, 54). The short spacers between the zinc-binding residues support a rather rigid coordination shell around the catalytic zinc ion in MMPs. Such structural rigidity was observed by our EXAFS results around the catalytic zinc ion in human gelatinase B. The three Zn-N(His) contributions could be fitted by a single theoretical Zn-N path in both pro- and activated enzymes throughout our EXAFS analysis.

These results raise the possibility that the tight binding of the three histidine ligands to the zinc ion is required for stabilization of the overall conformation of the active site protein

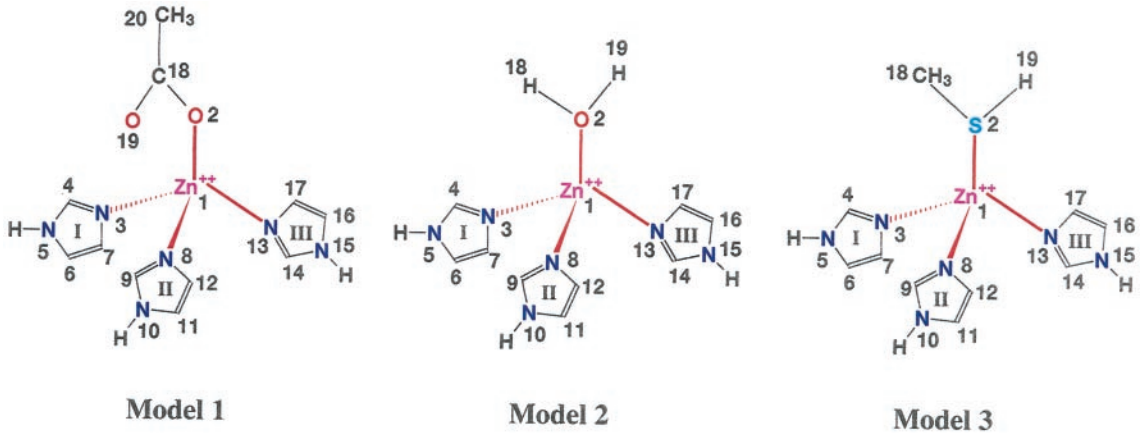

SCHEME 1. **Schematic presentation of the model molecules that were used for DFT calculations.** The schematic drawing is based on the optimized structures that were generated for the quantum mechanics calculations. The *symbols* and *numbers* designate the different atoms.

TABLE II
Summary of DFT calculations
Quantum chemistry calculation results of the optimization structures of the model molecules (see Scheme 1).

	Model 1	Model 2	Model 3	Ace[a]	Water[a]	MeSH[a]
Bond lengths (Å)						
1–2	2.012	2.091	2.498			
1–3	2.029	1.985	1.991			
1–8	2.029	1.980	1.995			
1–13	2.079	1.984	1.993			
1–19	2.345					
2–18	1.286	0.973	1.349	1.257	0.969	1.351
2–19		0.973	1.841		0.969	1.836
18–19	1.261			1.256		
18–20	1.509			1.576		
Bond angles and torsion angles (°)						
2–1-3	116.5	110.3	111.9			
2–1-8	116.2	110.3	108.5			
2–1-17	93.4	102.0	110.2			
1–2-18	96.8	121.8	112.9			
2–18-19	120.3			129.8		
18–2-19		106.7	98.5		103.7	96.9
3–1-2–8	145.8	120.2	124.9			
8–1-2–17	107.3	119.3	117.3			
3–1-2–18	73.0	−7.8	52.1			
1–2-18–19	−0.2					
Atomic charges (Q/e)						
1	0.938	0.989	0.899			
2	−0.600	−0.789	−0.035	−0.640	−0.774	−0.08
18	0.616	0.477	0.604	0.521	0.387	−0.577
19	−0.579	0.478	0.172	−0.639	0.387	0.095
20	−0.523			−0.502		
Total atomic charges (Q/e)						
Zn	0.938	0.989	0.899			
Ace	−0.531			−1.000		
Water		0.165			0.000	
Mesh			0.251			0.000
Thermodynamic parameters						
E_t (a.u.)[b]	−2686.25	−2533.85	−2896.13	−228.50	−76.41	−438.70
E_{Them} (kcal/mol)	184.75	166.49	182.68	33.09	15.06	31.38
S (cal/mol · K^{-1})	161.81	148.11	159.71	69.00	46.52	60.52
ΔE_t (kcal/mol)[c]	−194.53	0.0	6.28			
ΔE_{Them} (kcal/mol)[c]	0.23	0.0	−0.13			
ΔH (kcal/mol)[c]	−194.3	0.0	6.15			
ΔS (cal/mol · k^{-1})[c]	−8.78	0.0	−2.4			
ΔG (kcal/mol)[c]	−191.68	0.0	6.87			

[a] Ace, acetate; Water, H_2O; MeSH, CH_2SH; Im, imidazole.
[b] 1 a.u., 627.51 kcal/mol.
[c] The thermodynamic parameters were calculated using following the equations, Model 2 (C2) + Ace(L1) = Model 1 (C1) + water(L2); Model 2 (C2) + MeSH(L1) = Model β(C1) + water(L2); $\Delta E = E_t(\text{C1}) + E_t(\text{L2}) - E_t(\text{C2}) - E_t(\text{L1})$; $\Delta E_{\text{therm}} = E_{\text{therm}}(\text{C1}) + E_{\text{therm}}(\text{L2}) - \text{E}_{\text{therm}}(\text{C2}) - E_{\text{therm}}(\text{L1})$; $\Delta S = S(\text{C1}) + S(\text{L2}) - S(\text{C2}) - S(\text{L1})$; and $\Delta H = \Delta E + \Delta E_{\text{therm}}$, $\Delta H = \Delta H - T\Delta S$.

residues after the cleavage of the propeptide. In this case, the zinc-bound water in the activated enzyme may be poised for displacement by a substrate molecule (40). Exposure of the catalytic zinc ion to the surface in a rather fixed coordination (in the activated enzyme) may allow the enzyme catalysis to proceed without major change of the protein residues.

Comparison of the relative stability and energetics of acetate, water, and methane thiol at the fourth ligand position of the zinc ion by DFT calculations reveals an interesting trend of the binding affinities. As shown in Table II, the carboxylate group exhibits stronger binding to the zinc ion than water and methane thiol ligands.

This sequence can be used to explain the relationship between the enzyme activity of MMPs and the exogenous ligand. The function of the zinc ion in MMP seems to play a key role in both substrate binding and in catalysis. The sequence of these catalytic events may be governed by the identity of exogenous ligands.

The binding of water to the zinc ion in the simulated catalytic zinc site of MMPs is weak. The small size of a water molecule and its liability suggest that the coordination sphere of zinc can accommodate more than one exogenous ligand, which may be a substrate molecule. Moreover, the water molecule is more active as a nucleophile after binding to the zinc ion because the negative atomic charge increased after binding to the zinc ion (Table II). Yet only a moderate change in the total atomic charge of the zinc ion is observed upon the binding of water and the methane thiol ligand. These results are in good agreement with the relatively small edge shift to lower energy in the raw EXAFS data, which was observed upon activation of human gelatinase B. The shift in edge energy indicates the electronic shielding effect of the zinc ion in the various states of the enzyme. The moderate change of the activated enzyme spectra to a lower energy may indicate that the electron donor capabilities of an oxygen from water or sulfur from cysteine ligand at the catalytic zinc ion are similar. Our results support the mechanism scheme proposed by Matthews (56) and Lovejoy *et al.* (13) for thermolysin and human fibroblast collagenase. The binding of a water molecule at the activated enzyme provides a central intermediate in the catalytic process. In this mechanistic scheme, the water molecule attacks the carbonyl of the scissile bond and initiates proton transfer by donation of a proton to the Glu residue, which eventually facilitates the cleavage of the peptide bond.

In contrast, the acetate group binds the catalytic zinc ion too strongly, thus forming a tight coordination shell around the

zinc ion, which may decrease the ability of the enzyme to catalyze the substrate hydrolysis. A carboxylate group can coordinate to a zinc ion in two different ways as follows: a monodentate or a bidentate configuration that results in 4- and 5-fold coordinations of the zinc ion. According to the optimized geometry of model 1 (Scheme 1), we can regard bond Zn-1—O-19 as a partial coordination bond. In a way different from Ryde's calculation (51), we optimized the geometry of model 1 without any constraint (Ryde optimized this structure in monodentate and bidentate geometries by constraining the Zn-1—O-2—C-18 angle as 120 and 90°, respectively). The optimized geometry of model 1 gives the bond angle of Zn-1—O-2—C-18 as 96.8°, which is between the region of Ryde's constraint of 120 and 90° for monodentate and bidentate configurations, respectively. We therefore suggest that in active enzymes of MMPs, aspartate or glutamate may coordinate with Zn^{2+} in a way between monodentate and bidentate, and the coordination number could be between four and five.

In addition, the acetate ligand acts as a powerful zinc-binding functional group as was also shown by Ryde (51) and therefore may be considered as a good inhibitor for MMPs. This may account for the extensive studies of carboxylate-based MMP inhibitors.

REFERENCES

1. Birkedal-Hansen, H. (1995) *Curr. Opin. Cell Biol.* **7,** 728–735
2. Massova, I., Kotra, L. P., Fridman, R., and Mobashery, S. (1998) *FASEB J.* **12,** 1075–1095
3. Kiyama, R., Tamura, Y., Watanabe, F., Tsuzuki, H., Ohtani, M., and Yodo, M. (1999) *J. Med. Chem.* **42,** 1723–1738
4. Matrisian, L. M. (1990) *Trends Genet.* **6,** 121–125
5. Werb, Z. (1997) *Cell* **91,** 439–442
6. Shapiro, S. D. (1998) *Curr. Opin. Cell Biol.* **10,** 602–608
7. Nagase, H., and Woessner, J. F., Jr. (1999) *J. Biol. Chem.* **274,** 21491–21494
8. Van Wart, H. E., and Birkedal-Hansen, H. (1990) *Proc. Natl. Acad. Sci. U. S. A.* **87,** 5578–5582
9. Becker, J. W., Marcy, A. I., Rokosz, L. L., Axel, M. G., Burbaum, J. J., Fitzgerald, P. M., Cameron, P. M., Esser, C. K., Hermes, J. D., and Springer, J. P. (1995) *Protein Sci.* **4,** 1966–1976
10. Olson, M. W., Gervasi, D. C., Mobashery, S., and Fridman, R. (1997) *J. Biol. Chem.* **272,** 29975–29983
11. Lovejoy, B., Cleasby, A., Hassell, A. M., Longley, K., Luther, M. A., Weigl, D., McGeehan, G., McElroy, A. B., Drewry, D., Lambert, M. H., and Jordan, S. R. (1994) *Science* **263,** 375–377
12. Bode, W., Reinemer, P., Huber, R., Kleine, T., Schnierer, S., and Tschesche, H. (1994) *EMBO J.* **13,** 1263–1269
13. Lovejoy, B., Hassell, A. M., Luther, M. A., Weigl, D., and Jordan, S. R. (1994) *Biochemistry* **33,** 8207–8217
14. Gomis-Ruth, F. X., Maskos, K., Betz, M., Bergner, A., Huber, R., Suzuki, K., Yoshida, N., Nagase, H., Brew, K., Bourenkov, G. P., Bartunik, H., and Bode, W. (1997) *Nature* **389,** 77–81
15. Grams, F., Crimmin, M., Hinnes, L., Huxley, P., Pieper, M., Tschesche, H., and Bode, W. (1995) *Biochemistry* **34,** 14012–14020
16. Li, J., Brick, P., MC, O. H., Skarzynski, T., Lloyd, L. F., Curry, V. A., Clark, I. M., Bigg, H. F., Hazleman, B. L., Cawston, T. E., and Blow, D. M. (1995) *Structure* **3,** 541–549
17. Bode, W., Fernandez-Catalan, C., Tschesche, H., Grams, F., Nagase, H., and Maskos, K. (1999) *Cell Mol. Life Sci.* **55,** 639–652
18. Soler, D., Nomizu, T., Brown, W. E., Chen, M., Ye, Q.-Z., Van-Wart, H. E., and Auld, D. S. (1994) *Biochem. Cell Biol.* **201,** 917–923
19. Salow, S., Marcy, A. L., Cuca, G. C., Smith, C. K., Kopka, I. E., Hagmann, W. K., and Hermes, J. D. (1992) *Biochemistry* **31,** 4535–4540
20. Henning, B. (1995) *Curr. Opin. Cell Biol.* **7,** 728–725
21. Willenbrock, F., Murphy, G., Phillips, I. R., and Brocklehurst, K. (1995) *FEBS Lett.* **358,** 189–192
22. Morgunova, E., Tuuttila, A., Bergmann, U., Isupov, M., Lindqvist, Y., Schneider, G., and Tryggvason, K. (1999) *Science* **284,** 1667–1670
23. Dubois, B., Opdenakker, G., and Carton, H. (1999) *Acta Neurol. Belg.* **99,** 53–56
24. Masure, S., Proost, P., Van Damme, J., and Opdenakker, G. (1991) *Eur. J. Biochem.* **198,** 391–398
25. Opdenakker, G., Masure, S., Grillet, B., and Van Damme, J. (1991) *Lymphokine Cytokine Res.* **10,** 317–324
26. Gijbels, K., Masure, S., Carton, H., and Opdenakker, G. (1992) *J. Neuroimmunol.* **41,** 29–34
27. Opdenakker, G., and Van Damme, J. (1994) *Immunol. Today* **15,** 103–104
28. Liotta, L. A., Rao, C. N., and Barsky, S. H. (1983) *Lab. Invest.* **49,** 636–649
29. Rao, J., Steck, P. A., Mohanam, S., Stetler-Stevenson, W., Liotta, L. A., and Sawaya, R. (1993) *Cancer Res.* **53,** 2208–2211
30. Coussens, L. M., and Werb, Z. (1996) *Chem. Biol.* **3,** 895–904
31. Rudd, P., Mattu, T. S., Masure, S., Bratt, T., Van den Steen, P., Wornald, M. R., Kustner, B., Harvery, D. J., Borregaard, N., Dwek, R., and Opdenakker, G. (1999) *Biochemistry* **38,** 13937–13950
32. Norga, K., Grillet, B., Masure, S., Paemen, L., and Opdenakker, G. (1996) *Clin. Rheumatol.* **15,** 31–34
33. Van den Steen, P., Rudd, P. M., Proost, P., Martens, E., Paemen, L., Kuster, B., van Damme, J., Dwek, R. A., and Opdenakker, G. (1998) *Biochim. Biophys. Acta* **1425,** 587–598
34. Wuyts, A., Govaerts, C., Struyf, S., Lenaerts, J.-P., Put, W., Conings, R., Proost, P., and Van Damme, J. (1999) *Eur. J. Biochem.* **260,** 421–429
35. Strong, R. K., Bratt, T., Cowland, J. B., Borregaard, N., Wiberg, F. C., and Ewald, A. J. (1998) *Acta Crystallogr. Sect. D Biol. Crystallogr.* **54,** 93–95
36. Bradford, M. M. (1976) *Anal. Biochem.* **72,** 248–254
37. Knight, C. G., Willenbrock, F., and Murphy, G. (1992) *FEBS Lett.* **296,** 263–266
38. Masure, S., Billiau, A., Van Damme, J., and Opdenakker, G. (1990) *Biochim. Biophys. Acta* **1054,** 317–325
39. Stern, E. A., Newville, M., Ravel, B., Yacoby, Y., and Haskel, D. (1995) *Phys. Rev. B.* **208/209,** 117–122
40. Vallee, B. L., and Auld, D. S. (1990) *Proc. Natl. Acad. Sci. U. S. A.* **87,** 220–224
41. Rehr, J. J., Mustre, de leon, J., Zabinsky, S. I., and Albers, R. C. (1991) *J. Am. Chem. Soc.* **113,** 5135–5138
42. Zabinsky, S. I., Rehr, J. J., Ankudinov, A., Albers, R. C., and Eller, M. J. (1995) *Phys. Rev. B.* **52,** 2995–2999
43. Deleted in proof
44. Frisch, M. G., Trucks, G. W., H. B., Schlegel, G. E., Scuseria, M. A., Robb, J. R., Cheeseman, V. G., Zakrzewski, J. A., Montgomery, R. E., Jr., Stratmann, J. C., Burant, S., Dapprich, J. M., Millam, A. D., Daniels, K. N., Kudin, M. C., Strain, O., Farkas, J., Tomasi, V., Barone, M., *et al.* (1998) Gaussian, Inc., Pittsburgh, PA
45. Scott, R. A. (1985) *Methods Enzymol.* **117,** 414–458
46. Kleifeld, O., Frenkel, A., Bogin, O., Eisenstein, M., Brumfeld, V., Burstein, Y., and Sagi, I. (2000) *Biochemistry* **39,** 7702–7711
47. Stocker, W., and Bode, W. (1995) *Curr. Opin. Struct. Biol.* **5,** 383–390
48. Parr, R. G., and Yang, W. (1989) *Density-functional Theory of Atoms and Molecules,* 2nd Ed., Oxford University Press, Oxford
49. Becke, A. D. (1993) *J. Chem. Phys.* **98,** 5648–5652
50. Holthausen, M., Mohr, M., and Koch, W. (1995) *Chem. Phys. Lett.* **240,** 245–252
51. Ryde, U. (1999) *Biophys. J.* **77,** 2777–2787
52. Bauschlicher, C. W. (1995) *Chem. Phys. Lett.* **246,** 40–44
53. Ricca, A., and Bauschlicher, C. W. (1995) *Theor. Chim. Acta* **92,** 123–131
54. Borkakoti, N. (1998) *Prog. Biophys. Mol. Biol.* **70,** 73–94
55. Springman, E. B., Nagase, H., Birkedal-Hansen, H., and Van Wart, H. E. (1995) *Biochemistry* **34,** 15713–15720
56. Matthews, B. W. (1988) *Acc. Chem. Res.* **21,** 333–340
57. Springman, E. B., Angleton, E. L., Birkedal-Hansen, H., and Van Wart, H. E. (1990) *Proc. Natl. Acad. Sci. U. S. A.* **87,** 364–368